

Fault Location in Hybrid AC/DC Transmission Grids Containing DERs and HVDC Lines

Cesar Galvez¹, Graduate Student Member, IEEE, and Ali Abur², Fellow, IEEE

Abstract—This paper introduces a new fault location method for hybrid AC/DC complex transmission grids containing Distributed Energy Resources (DERs) and Modular Multilevel Converter-High Voltage Direct Current (HVDC) lines. Digital Fault Recorders (DFR) in the DC grid cannot observe faults occurring in the AC network and vice-versa. The proposed algorithm accurately locates faults irrespective of their location using a subset of DFRs selected by a K-means clustering method. The algorithm is tested using an AC/DC complex transmission network formed by merging the modified IEEE 39 bus transmission system and the CIGRE B4 DC grid test systems under several fault conditions using EMTP-RV and MATLAB as simulation tools.

Index Terms—Fault location, AC and DC faults, traveling waves, discrete wavelet transform, K-means, tree network.

I. INTRODUCTION

PROVEN benefits of increased power transmission capacity, reactive and active power control flexibility, long distance transmission, low line loss, and facilitating access to remote distributed energy resources (DER) make HVDC networks overlaid on AC grids an attractive alternative. Moreover, high penetration of DERs connected via Inverter Based Power Sources (IBPS) creates new challenges in protection and fault location in AC/DC networks. Impedance-based conventional fault location methods have limitations due to unknown fault impedance [1], asymmetry of lines, and the fault ride-through (FRT) requirements of renewables imposed by grid codes [2]. On the other hand, the traveling wave (TW) based methods lack such limitations [3], [4], but need to address other issues such as non-symmetric or mixed-phase lines and cables, synchronization-time or measurement errors, differentiating fault transients from capacitor or load switching, and attenuation of signals by power transformers. Fault location methods using the TW approach is already used in DC transmission projects [5], [6]. Traditional TW methods for fault location in DC systems utilize either double-ended or single-ended measurements. Single-ended approaches compared with

double-ended methods do not need communication devices and Global Positioning Systems (GPS) [5], [7]. The single-ended method utilizes the time differences between two consecutive wave fronts of fault-generated traveling waves in order to determine the precise fault distance. Thereby, capturing the wave front is critical to obtain the right precision in single-ended methods [6], [8]. The high resolution of wavelet transform (WT) is used to capture the two wave fronts with high precision [7], [9]. A single-ended case for DC lines is presented in [10], but it was limited to strictly radial networks. Overall, single-ended methods tend to lose precision in locating faults in multi-terminal and meshed networks. On the other hand, two-terminal fault location methods are precise and can be used in any type of network topology. The technique presented in [11] can locate faults in meshed DC micro-grids, using the Pearson correlation coefficient and a user specified detection threshold which is not always easy to choose. It also requires a large number of measurement points to estimate the fault distance for a simple meshed network. In [12], the fault current is registered and compared with a threshold. Although, this process is simple, it is challenging to establish a suitable threshold. In [13], a minimum detector placement and fault location based on two invariant graphs are presented, but application for large grids and impact of real disturbances in power grids are not provided.

The above methods contribute to the fault location in AC and DC power networks but with some limitations. In general, fault location capability of the previous methods is diminished in complex DC meshed transmission networks containing line-cable hybrid configurations. Moreover, they are designed either only for AC or only for DC networks, but none can locate faults in mixed AC/DC systems. In case of a fault, it is important and useful to quickly know if the fault occurs in the AC or DC network and its exact location. Our early work [14] showed that faults could be located in meshed distribution networks by placing DFRs in lateral terminals. Despite its effectiveness, the number of required DFRs increases with system size and complexity.

This paper presents a more efficient alternative approach and introduces a new Digital Fault Recorder (DFR) placement method to successfully implement it. The proposed method can accurately locate faults in AC/DC networks regardless of their location in AC or DC network and the use of TWs current limiting reactors or unknown fault impedances will have no impact on the performance of the proposed method. It is noted that the method is an off-line application which uses synchronized DFRs to capture the time-of-arrivals (ToAs) extracted from the

Manuscript received 15 April 2022; revised 5 January 2023 and 11 February 2023; accepted 18 February 2023. Date of publication 22 February 2023; date of current version 26 December 2023. This work was supported in part by the Engineering Research Center Program of the National Science Foundation and the Department of Energy under NSF Award EEC-1041877 and in part by CURENT Industry Partnership Program. Paper no. TPWRS-00545-2022. (Corresponding author: Ali Abur.)

The authors are with the Electrical and Computer Engineering Department, Northeastern University, Boston, MA 02151 USA (e-mail: galvez-nunez.c@husky.neu.edu; abur@ece.neu.edu).

Color versions of one or more figures in this article are available at <https://doi.org/10.1109/TPWRS.2023.3247661>.

Digital Object Identifier 10.1109/TPWRS.2023.3247661

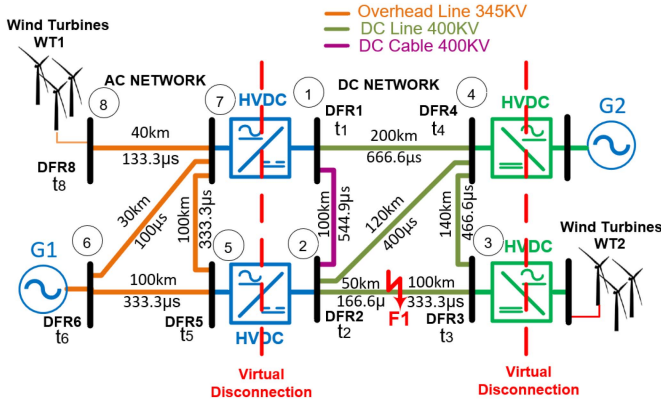


Fig. 1. Small hybrid AC/DC transmission system.

fault initiated traveling waves (TW) to estimate the accurate fault location. In case of an AC/DC network, the proposed method uses a small subset of available DFRs selected using K-Means clustering. The selected DFRs are then used to identify the faulted network and determine the fault-closest bus, which is identified as the one yielding the minimum ℓ_2 norm. The edges incident to the closest bus to the fault are then selected, but since the faulted edge is unknown, the shortest routes from fault to clustered DFRs for each incident edge are modeled as a weighted directed tree. This representation facilitates forming of ToA matrices at each terminal bus of incident edge and provides redundancy in the fault distance estimation, making the proposed method robust against bad data and time-synchronization errors. Finally, all possible ToA pairs are formed and using a new two-terminal fault location method, the fault location is accurately estimated.

II. PROBLEM FORMULATION

A small hybrid AC/DC transmission system shown in Fig. 1 will be used to describe the details of the proposed fault location method. The model contains a 345 kV AC transmission system connected via two MMC-HVDC to a 400 kV DC transmission system. Besides, a wind turbine (WT2) and a synchronous generator (G2) provide power to the DC system via two MMC-HVDC converters. Note that the DC system also has a cable section connecting the buses 1-2. Consider a fault F1 occurring at 50 km from bus 2 along the 400 kV DC line as shown in Fig. 1. While the fault location method proposed will be illustrated for meshed DC systems, it can readily be used for AC transmission systems as will be shown in the simulation section.

A. Optimal DFR Placement (ODP)

Initially, the AC and DC networks in the small AC/DC transmission system are virtually disconnected as shown in Fig. 1. Therefore, fault identification and optimal DFR placement (ODP) are carried out separately for the AC and DC networks, each of which is represented as undirected weighted graphs as shown in Figs. 2 and 3. Each graph is then denoted by $G = (v, \epsilon, \tau)$, where v is the set of buses or nodes with size n , ϵ is the set of edges or lines with size L ($L \geq n - 1$), and

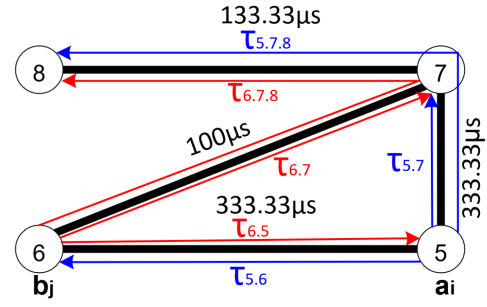


Fig. 2. Weighted undirected graph of the AC network.

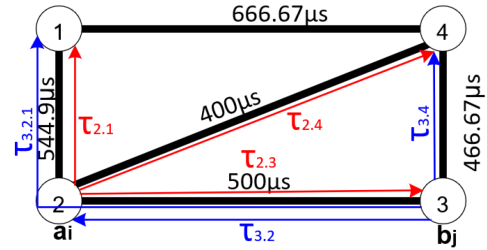


Fig. 3. Weighted undirected graph of the DC network.

τ is the set of weights given by the traveling times τ_i (μs) of each edge i , where ($\tau_i = l_i/V_i = l_i\sqrt{L_i.C_i}$), l_i being the line length, V_i the TW speed for each edge i , and C_i and L_i are conductor capacitance and inductance per unit length for each edge i . The new optimal DFR placement (ODP) approach, which ensures the identification of any fault in the system using a minimum number of DFRs will be described first. The ODP method follows the same approach for AC and DC networks as will be shown in the sequel. When a fault occurs on a line-cable hybrid network, fault-generated traveling waves propagate from the fault to system buses following the shortest traveling time routes. Now, let us select any branch from the AC network to explain the optimal DFR placement (ODP) approach proposed in this work. Considering branch 5-6 as the section in evaluation, the shortest travel times from its terminal buses 5 (a_i) and 6 (b_j) to all system buses n (red and blue arrows respectively) can be computed as shown in Fig. 2. Note that if a fault occurred along branch 5-6, the shortest travel times $\tau_{5,6}$ and $\tau_{6,5}$ would be the only two needed to estimate the fault distance. Hence, a binary vector for each terminal bus of branch 5-6 can be computed using the conditions (1) and (2) as illustrated below.

$$T_{(a_i,n)} = \begin{cases} 1 & \text{If there is at least a shortest traveling} \\ & \text{time from bus "a}_i\text{" to system buses} \\ & \text{"n" containing bus "b}_j\text{"} \\ 0 & \text{Otherwise} \end{cases} \quad (1)$$

$$T_{(b_j,n)} = \begin{cases} 1 & \text{If there is at least a shortest traveling} \\ & \text{time from bus "b}_j\text{" to system buses} \\ & \text{"n" containing bus "a}_i\text{"} \\ 0 & \text{Otherwise} \end{cases} \quad (2)$$

where, a_i and b_j are the terminal buses of network branches and n represents the system buses. The binary vectors for buses 5 and 6 will then be obtained as follows:

$$T_{(a_5,n)} = a_5 \begin{bmatrix} 5 & 6 & 7 & 8 \\ 0 & 1 & 0 & 0 \end{bmatrix}$$

$$T_{(b_6,n)} = b_6 \begin{bmatrix} 5 & 6 & 7 & 8 \\ 1 & 0 & 0 & 0 \end{bmatrix}$$

Repeating the procedure for all other system branches (5-7, 6-7, 7-8), the following $2L \times n$ binary matrix T can be formed, where L is the number of branches:

$$T = \begin{matrix} a_5 \\ b_6 \\ a_5 \\ b_7 \\ a_6 \\ b_7 \\ a_7 \\ b_8 \end{matrix} \begin{bmatrix} 5 & 6 & 7 & 8 \\ 0 & 1 & 0 & 0 \\ 1 & 0 & 0 & 0 \\ 0 & 0 & 1 & 1 \\ 1 & 0 & 0 & 0 \\ 0 & 0 & 1 & 1 \\ 0 & 1 & 0 & 0 \\ 0 & 0 & 0 & 1 \\ 1 & 1 & 1 & 0 \end{bmatrix} \quad (3)$$

Once matrix T is formed, the ODP problem can be formulated for a system with n buses and L branches as follows:

$$\text{minimize } \sum_{k=1}^n w_k \cdot x_k \quad (4)$$

$$\text{s.t. } [T][X] \geq b \quad (5)$$

where,

$$T = [T]_{2L \times n}$$

$$X = [x_1, x_2, x_3, \dots, x_n]_{n \times 1}^T$$

$$b = [1, 1, 1, \dots, 1]_{2L \times 1}^T$$

Where, x_k will be 1 if a DFR is installed at bus k or 0 otherwise, and w_k represents the installation cost of DFR_k at bus k . Assuming that the cost of installation for all the DFRs is the same, the optimal DFR placement (ODP) for the AC transmission network of Fig. 2 will be given by:

$$X = [1 \ 1 \ 0 \ 1]^T$$

This implies that buses 5, 6, and 8 are the optimal locations for installing DFRs in the AC network. Now, applying the ODP method to the DC network of Fig. 3 will yield the $2L \times n$ binary matrix T given below in (6), where L and n are the number of branches and buses of the DC network. The red and blue arrows in Fig. 3 correspond only to the processing of branch 2-3. Repeating the process for all other branches (1-2, 1-4, 2-4,

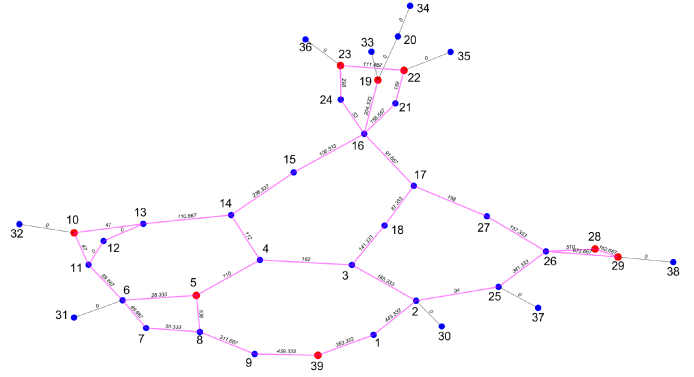


Fig. 4. Optimal DFR placement (ODP) for IEEE 39-bus system.

4-3) will yield the complete matrix T below:

$$T = \begin{matrix} a_1 \\ b_2 \\ a_1 \\ b_4 \\ a_2 \\ b_4 \\ a_2 \\ b_3 \\ b_3 \end{matrix} \begin{bmatrix} 1 & 2 & 3 & 4 \\ 0 & 1 & 1 & 0 \\ 1 & 0 & 0 & 0 \\ 0 & 0 & 0 & 1 \\ 1 & 0 & 0 & 0 \\ 0 & 0 & 0 & 1 \\ 0 & 1 & 0 & 0 \\ 0 & 0 & 1 & 0 \\ 1 & 1 & 0 & 0 \\ 0 & 0 & 1 & 0 \\ 0 & 0 & 0 & 1 \end{bmatrix} \quad (6)$$

The optimal DFR locations for the DC network will then be given by:

$$X = [1 \ 1 \ 1 \ 1]^T$$

This implies that buses 1, 2, 3, and 4 are optimal locations for installing DFRs in the DC system. Therefore, seven DFRs (three AC DFRs and four DC DFRs) will be required to make any fault identifiable in the small hybrid AC/DC transmission system of Fig. 1. Next, the same procedure will be applied for the larger IEEE 39-bus system [15] shown in Fig. 4. The resulting optimal DFR locations are given below:

$$ODP = [5 \ 10 \ 19 \ 22 \ 23 \ 28 \ 29 \ 39]$$

The bus locations of these eight DFRs determined by ODP are also marked in red in Fig. 4. Note that this example only involves an AC system which contains power transformers radially connected to the network. Therefore, these laterals are represented with line lengths of zero and are not included in the optimization problem. If a fault occurs in any of the power transformers, the proposed algorithm will detect it at the bus where the faulted transformer connects to the network.

B. Initial Considerations

AC and DC transmission lines are modeled using the Frequency-Dependent (FD) line model [16]. Three-phase AC voltage signals recorded by the DFRs are converted from phase to modal domain using Clarke's Transformation [17]. No such conversion is needed for the DC voltage signals. Discrete Wavelet Transforms (DWT) (with Daubechies2 as the mother wavelet (DB2) [18]) of the modal domain voltage waveforms

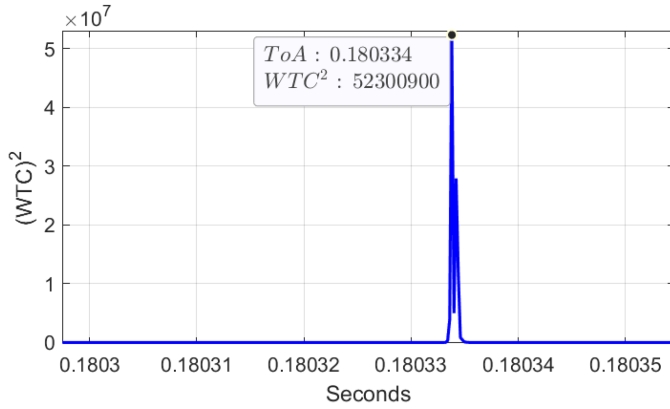


Fig. 5. WTC^2 captured by DFR3 for Fault F1 in DC network.

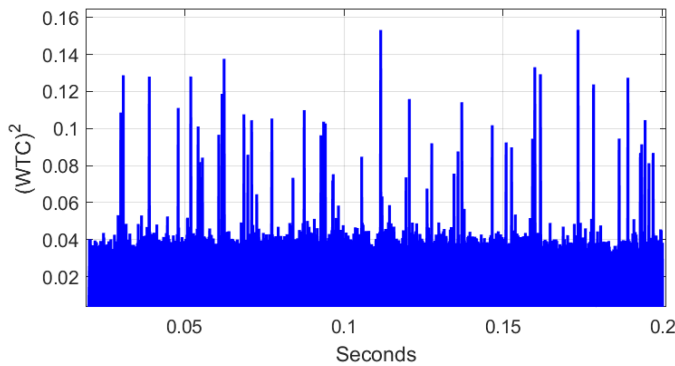


Fig. 6. WTC^2 captured by DFR5 for fault F1 in AC network.

are then calculated. Among the five computed wavelet-transform coefficients (WTCs), those at level 1 (D1) are then processed to determine ToAs due to their rich high-frequency content. Finally, to reduce the effect of noise, squares of WTCs are used as done also in [3].

C. Selecting a Subset of DFRs

Fault location in hybrid networks with the presence of power transformers and HVDCs is very challenging due to the ground connection of power transformer neutrals as well as the switching of converters in MMC-HVDCs, which attenuate and distort the TWs. For example, the TWs generated by a fault at F1 in Fig. 1 will be precisely captured by DFRs 1, 2, 3, and 4 due to their proximity to the F1 location in the DC system. On the other hand, the DFRs 5, 6, and 8 in the AC system will capture erroneous ToAs because HVDC converters act like filters distorting the fault-generated TWs when these pass through them. This is illustrated in Figs. 5 and 6 for fault F1, where DFR3 in DC network captured high magnitudes of WTC^2 , but DFR5 in AC network registered erroneous magnitudes close to zero as shown in Fig. 6. Hence, instead of using the entire set of DFRs, a subset of DFRs can be selected to determine the faulted network and estimate the accurate fault location. These DFRs are selected using K-Means clustering, which will display a cluster as shown in Fig. 7. The red cluster C_1 will contain the correct ToAs from DFRs located in the DC system, while ToAs from the blue cluster C_2 will be erroneous due to the distortion

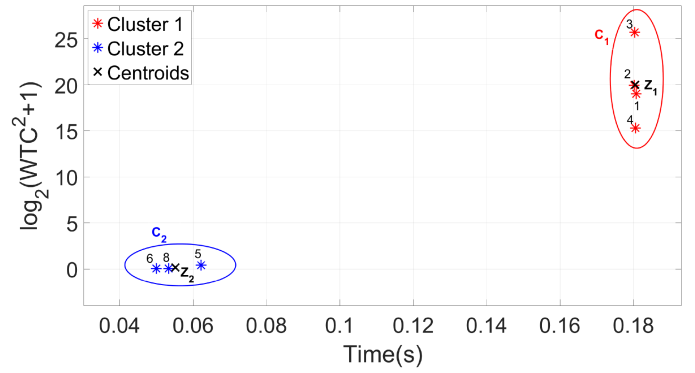


Fig. 7. K-Means cluster for identification of faulted system.

produced by the HVDC converters. The feature vector $x^{(i)}$ used by K-Means will be given by:

$$x^{(i)} = (t_i, \log_2(WTC_i^2 + 1)) \quad (7)$$

where:

$x^{(i)}$ is the feature vector for p DFRs, $i = 1, 2, \dots, p$.

t_i is the ToA recorded by DFR_i

WTC_i^2 is the magnitude of the squared Wavelet Transform Coefficient recorded by DFR_i .

Due to the WTC^2 magnitude differences between DFRs, logarithms of WTC_i^2 are used instead to better visualize clusters. Also, WTC^2 are replaced by $(1 + WTC^2)$ before taking their logarithms to avoid negative values corresponding to erroneous (close to zero) magnitudes captured by some DFRs. Logarithms will all be positive for the clusters as displayed in Fig. 7. The K-Means algorithm [19] is then used to determine suitable assignments of clusters (C_1, \dots, C_k), and the representatives (Centroids) of each of the k clusters (z_1, \dots, z_k). K-Means requires as input the cluster number k , which can be determined using the well-known elbow method [19]. Given the set of feature vector S_n for p DFRs and the number of clusters k , the K-Means algorithm performs the following steps:

$$S_n = \{x^{(i)} | i = 1, 2, \dots, p\} \quad (8)$$

- 1) Randomly select z_1, \dots, z_k , for $j = 1, \dots, k$
- 2) Iterate
 - a) Given z_1, \dots, z_k , assign each feature vector $x^{(i)}$ to closest z_j , so that.

$$Cost(z_1, \dots, z_k) = \sum_{i=1}^p \min_{j=1, \dots, K} \|x^{(i)} - z_j\| \quad (9)$$

- b) Given C_1, \dots, C_k determine the best representatives z_1, \dots, z_k , such that.

$$z_j = \operatorname{argmin}_z \sum_{i \in C_j} \|x^{(i)} - z\|^2 \quad (10)$$

where:

p is DFR number in DC and AC networks, for $i = 1, \dots, p$.

k is the cluster number, for $j = 1, \dots, k$.

C_j are the clusters, for $j = 1, \dots, k$.

In the case of F1 fault at Fig. 1, using K-Means will yield two clusters C_1 and C_2 and their best representatives or centroids z_1 and z_2 for each cluster as depicted in Fig. 7. The cluster C_1 formed by DFR_i , $i = 1, 2, 3$, and 4, and placed in DC network will then capture the correct ToAs to compute the precise fault distance. Hence, the fault location computations will be based on the measurements by these four DFRs only.

D. Identifying the Fault-Closest Bus

Using K-Means clustering in the small hybrid AC/DC transmission system of Fig. 1 will identify the DC network as the faulted network. Hence, only the DC network will be used to determine the fault-closest bus and estimate accurate fault location. Considering the F1 fault of Fig. 1 close to bus 2 is recorded first by DFR2. Hence, DFR2 will be the reference DFR in the identification of fault-closest bus. The ToAs registered by clustered DFRs from previous step at buses 1, 2, 3, and 4 are then stored as:

$$ToA_1^T = [t_1 \quad t_2 \quad t_3 \quad t_4] \quad (11)$$

Using bus 2 as the reference a relative ToA_2 vector with respect to DFR2 can be formed as:

$$ToA_2^T = [t_1 - t_2 \quad t_2 - t_2 \quad t_3 - t_2 \quad t_4 - t_2] \quad (12)$$

Now, consider the $p \times n$ matrix τ_A formed by traveling times between buses:

$$\tau_A = \begin{matrix} & \begin{matrix} 1 & 2 & \dots & n-1 & n \end{matrix} \\ \begin{matrix} 1 \\ 2 \\ 3 \\ \cdot \\ \cdot \\ p \end{matrix} & \begin{bmatrix} 0 & \tau_{1,2} & \dots & \tau_{1,(n-1)} & \tau_{1,n} \\ \tau_{2,1} & 0 & \dots & \tau_{2,(n-1)} & \tau_{2,n} \\ \tau_{3,1} & \tau_{3,2} & \dots & \tau_{3,(n-1)} & \tau_{3,n} \\ \cdot & \cdot & \dots & \cdot & \cdot \\ \cdot & \cdot & \dots & \cdot & \cdot \\ \tau_{p,1} & \tau_{p,2} & \dots & \tau_{p,(n-1)} & \tau_{p,n} \end{bmatrix} \end{matrix} \quad (13)$$

where p is the number of buses with DFRs and n is the number of buses in the network. Besides, let the $p \times p$ matrix D be defined as:

$$D = \begin{matrix} & \begin{matrix} 1 & k & 3 & \dots & p-1 & p \end{matrix} \\ \begin{matrix} 1 \\ k \\ 3 \\ \cdot \\ \cdot \\ p \end{matrix} & \begin{bmatrix} 1 & -1 & 0 & \dots & 0 & 0 \\ 0 & 0 & 0 & \dots & 0 & 0 \\ 0 & -1 & 1 & \dots & 0 & 0 \\ \cdot & \cdot & \cdot & \dots & \cdot & \cdot \\ \cdot & \cdot & \cdot & \dots & \cdot & \cdot \\ 0 & -1 & 0 & \dots & 0 & 1 \end{bmatrix} \end{matrix} \quad (14)$$

Where k corresponds to the reference DFR and column k contains all “-1”s except for the k row which is 0. Taking the product of D and τ_A , a reduced relative ToA matrix τ_{red} can be obtained:

$$\tau_{red} = \begin{matrix} D & \times & \tau_A \\ p \times p & & p \times n \end{matrix} \quad (15)$$

Now, subtracting the ToA_2 vector of (12) from every column of τ_{red} , a travel time mismatch matrix $\Delta\tau$ is obtained as:

$$\Delta\tau = \begin{matrix} \tau_{red} & - & [ToA_2] \\ p \times n & & p \times n \end{matrix} = \begin{matrix} [1 & 1 & 1 & \dots & 1] \\ p \times 1 & & 1 \times n \end{matrix} \quad (16)$$

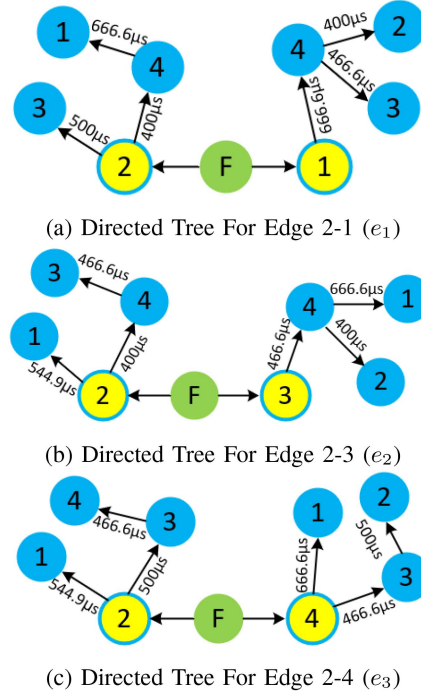


Fig. 8. Directed tree model for incident edges. (a) Directed tree for edge 2-1 (e_1). (b) Directed tree for edge 2-3 (e_2). (c) Directed tree for edge 2-4 (e_3).

The fault-closest bus j will then be given by the bus that minimizes the following:

$$\ell(j) = \min_j (\|\Delta\tau_j\|_2; j \in \{1, 2, \dots, n\}) \quad (17)$$

For the case of F1 fault at Fig. 1, $j = 2$ and $n = 4$. Note that only the four buses of DC network are included in the identification of the fault-closest bus 2 due to the selected DFRs are placed in the DC transmission network.

E. Determining the Accurate Fault Distance

The incident edges to the fault-closest bus 2 (2-1, 2-3, 2-4) of Fig. 3 must be evaluated in order to determine the faulted line section which will lead to the precise fault location. For the sake of illustration, consider the ToAs (ms) recorded by DFRs 1, 2, 3, and 4 for fault F1 to be 30.711, 30.166, 30.333, and 30.566, respectively. Then, the location of the fault will be determined as follows:

- 1) Form the weighted directed tree for each edge incident to the fault-closest bus. For the example in Fig. 1, the three directed trees corresponding to the edges 2-1, 2-3, and 2-4 are shown in Fig. 8. In Fig. 8, the unknown location of the fault F1 is highlighted by green in each incident edge; terminals of incident edges by yellow, and DFR locations by light blue. Also, light blue circled buses indicate presence of a DFR.
- 2) Determine the shortest traveling times to all p DFRs using (18) in Fig. 8 and assuming the fault at the fault-closest bus 2 and the faulted edge “ e_1 ” (2-1). Repeat this for edges “ e_2 ” (2-3) and “ e_3 ” (2-4) and save the results in a $p \times \varepsilon$

matrix τ_a . Repeat the same process assuming the fault is at the “other” terminals (1, 3, 4) of the faulted edge. Save the results in a $p \times \varepsilon$ matrix τ_b as shown below:

$$\tau_{(k,h)}^{(e_i)} = \sum_{j=1}^N \tau_j \quad (18)$$

$$\tau_a = \begin{matrix} & e_1 & e_2 & e_3 \\ \begin{matrix} 1 \\ 2 \\ 3 \\ 4 \end{matrix} & \begin{bmatrix} \tau_{1,2}^{e_1} & \tau_{1,2}^{e_2} & \tau_{1,2}^{e_3} \\ \tau_{2,2}^{e_1} & \tau_{2,2}^{e_2} & \tau_{2,2}^{e_3} \\ \tau_{3,2}^{e_1} & \tau_{3,2}^{e_2} & \tau_{3,2}^{e_3} \\ \tau_{4,2}^{e_1} & \tau_{4,2}^{e_2} & \tau_{4,2}^{e_3} \end{bmatrix} \end{matrix}$$

$$= \begin{matrix} & e_1 & e_2 & e_3 \\ \begin{matrix} 1 \\ 2 \\ 3 \\ 4 \end{matrix} & \begin{bmatrix} 1066.67 & 544.9 & 544.9 \\ 0 & 0 & 0 \\ 500 & 866.67 & 500 \\ 400 & 400 & 966.67 \end{bmatrix} \end{matrix}$$

$$\tau_b = \begin{matrix} & e_1 & e_2 & e_3 \\ \begin{matrix} 1 \\ 2 \\ 3 \\ 4 \end{matrix} & \begin{bmatrix} \tau_{1,1}^{e_1} & \tau_{1,3}^{e_2} & \tau_{1,4}^{e_3} \\ \tau_{2,1}^{e_1} & \tau_{2,3}^{e_2} & \tau_{2,4}^{e_3} \\ \tau_{3,1}^{e_1} & \tau_{3,3}^{e_2} & \tau_{3,4}^{e_3} \\ \tau_{4,1}^{e_1} & \tau_{4,3}^{e_2} & \tau_{4,4}^{e_3} \end{bmatrix} \end{matrix}$$

$$= \begin{matrix} & e_1 & e_2 & e_3 \\ \begin{matrix} 1 \\ 2 \\ 3 \\ 4 \end{matrix} & \begin{bmatrix} 0 & 1133.3 & 666.6 \\ 1066.6 & 866.67 & 966.6 \\ 1133.2 & 0 & 466.6 \\ 666.6 & 466.6 & 0 \end{bmatrix} \end{matrix}$$

where e_i , for $i = 1, 2, \dots, \varepsilon$, are the incident edges, $h = 1, 2, \dots, m$, correspond to terminal buses of incident lines, and $k = 1, 2, \dots, p$, are the DFR indices. τ_j is the traveling time for line section j along the shortest path from each terminal bus to the DFRs, and N is the number of line sections in the shortest path.

3) Form the t_a and t_b arrival time matrices as:

$$t_a = \begin{matrix} p \times \varepsilon \\ [ToA_1] \cdot \begin{matrix} 1 & 1 & 1 & \dots & 1 \\ p \times 1 & 1 \times \varepsilon & & & \end{matrix} \end{matrix} - \tau_a \quad (19)$$

$$t_b = \begin{matrix} p \times \varepsilon \\ [ToA_1] \cdot \begin{matrix} 1 & 1 & 1 & \dots & 1 \\ p \times 1 & 1 \times \varepsilon & & & \end{matrix} \end{matrix} - \tau_b \quad (20)$$

where ToA_1 is the vector containing ToAs of p DFRs. The matrices t_a and t_b are evaluated as below in order to find the correct ToAs corresponding to the shorter path between those from the two terminals of the incident edges to the DFRs:

$$t_a(k, i) = \begin{cases} 0 & \text{if } \tau_a(k, i) \geq \tau_b(k, i) \\ t_a(k, i) & \text{otherwise} \end{cases} \quad (21)$$

$$t_b(k, i) = \begin{cases} 0 & \text{if } \tau_b(k, i) \geq \tau_a(k, i) \\ t_b(k, i) & \text{otherwise} \end{cases} \quad (22)$$

where k and i are the row and column indices at each matrix. For the directed tree of Fig. 8, t_a and t_b will be

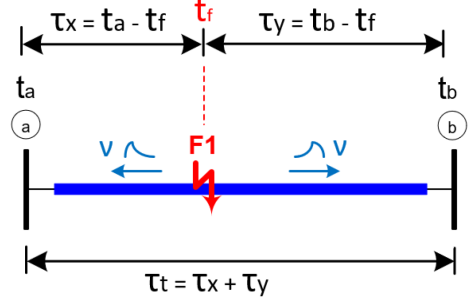


Fig. 9. Fault distance estimation.

given as:

$$t_a = \begin{matrix} & e_1 & e_2 & e_3 \\ \begin{matrix} 1 \\ 2 \\ 3 \\ 4 \end{matrix} & \begin{bmatrix} 0 & t_{a(1,2)} & t_{a(1,3)} \\ t_{a(2,1)} & t_{a(2,2)} & t_{a(2,3)} \\ t_{a(3,1)} & 0 & 0 \\ t_{a(4,1)} & t_{a(4,2)} & 0 \end{bmatrix} \end{matrix}$$

$$= \begin{matrix} & e_1 & e_2 & e_3 \\ \begin{matrix} 1 \\ 2 \\ 3 \\ 4 \end{matrix} & \begin{bmatrix} 0 & 30.167 & 30.167 \\ 30.167 & 30.167 & 30.167 \\ 29.833 & 0 & 0 \\ 30.167 & 30.167 & 0 \end{bmatrix} \end{matrix}$$

$$t_b = \begin{matrix} & e_1 & e_2 & e_3 \\ \begin{matrix} 1 \\ 2 \\ 3 \\ 4 \end{matrix} & \begin{bmatrix} t_{b(1,1)} & 0 & 0 \\ 0 & 0 & 0 \\ 0 & t_{b(3,2)} & t_{b(3,3)} \\ 0 & 0 & t_{b(4,3)} \end{bmatrix} \end{matrix}$$

$$= \begin{matrix} & e_1 & e_2 & e_3 \\ \begin{matrix} 1 \\ 2 \\ 3 \\ 4 \end{matrix} & \begin{bmatrix} 30.711 & 0 & 0 \\ 0 & 0 & 0 \\ 0 & 30.333 & 29.866 \\ 0 & 0 & 30.567 \end{bmatrix} \end{matrix}$$

Selecting the same columns corresponding to the edges “ e_i ”, $i = 1, 2, \dots, \varepsilon$, in t_a and t_b , form ToA pairs to compute the fault distance.

4) Compute the fault location vector X_D for each incident edge e_i . Let us use Fig. 9 to derive a new two-terminal fault location method. Assume that the correct ToA number (non-zero) in column e_i of t_a and t_b are “ q ” and “ v ” respectively. Hence, there will be $s = q \times v$, possible ToA pairs for $r = 1, 2, \dots, s$. Consider a fault F1 occurring at t_f along the line as indicated in Fig. 9. It can be shown that, given the actual travel time τ_t for the incident edge e_i , it is possible to solve for travel time $\tau_{x(r)}$ from F1 to the fault-closest bus as follows:

$$\tau_{x(r)} = \frac{1}{2} \left(t_{a_q}^{(e_i)} - t_{b_v}^{(e_i)} + \tau_t^{(e_i)} \right) \quad (23)$$

For the case of column e_1 in t_a and t_b , $q = 3$ and $v = 1$. Hence, $s = 3 \times 1 = 3$, for $r = 1, 2, 3$. The computation for column e_2 will yield the same number of ToA pairs as e_1 , but the computation for column e_3 will yield four ToA

TABLE I
FAULT LOCATION TABLE FOR FAULT F1 OF FIG. 1

Edge	t_a	t_b	τ_x	v_e	X_D	τ_e	τ_t	err_{τ_e}
2-1	30.167	30.712	0.02	183505	0.00	544.90	544.94	0.01
2-1	29.833	30.712	-166.83	183505	-30.61	878.60	544.94	61.23
2-1	30.167	30.712	0.02	183505	0.00	544.90	544.94	0.01
2-3	30.167	30.333	166.63	300000	49.99	166.73	500.00	66.65
2-3	30.167	30.333	166.63	300000	49.99	166.73	500.00	66.65
2-3	30.167	30.333	166.63	300000	49.99	166.73	500.00	66.65
2-4	30.167	29.867	350.00	300000	105.00	300.00	400.00	25.00
2-4	30.167	30.567	0.02	300000	0.00	399.97	400.00	0.01
2-4	30.167	29.867	350.00	300000	105.00	300.00	400.00	25.00
2-4	30.167	30.567	0.00	300000	0.00	400.00	400.00	0.00

pairs. Finally, taking the fault-closest bus as a reference, the fault distance $X_{(r)}$ for pairs s can be estimated as:

$$X_{(r)} = v_{(e_i)} \cdot \tau_{x(r)} \quad (24)$$

where $v_{(e_i)}$ is the TW speed for the edge e_i .

The computed fault distances $X_{(r)}$ are then stored in the fault location vector X_D .

$$X_D = [X_1 \quad X_2 \quad X_3 \quad \dots \quad X_{s-1} \quad X_s] \quad (25)$$

Note that X_D must be calculated for each incident edge e_i . For the case of Fig. 8, X_D must be estimated three times for e_1 , e_2 and e_3 using (23) and (24).

- The last step determines the accurate fault distance through the fault location table computation. The ToA pairs formed by combining the corresponding columns e_i in t_a and t_b are used in (23) and (24) to compute X_D for each incident edge e_i and populate the fault location Table I. Note that the actual travel time τ_t , and TW speed v_e for each incident edge e_i are known network parameters.

The incident edges 2-1, 2-3, and 2-4 correspond to the labels e_1 , e_2 and e_3 , respectively. As evident in Table I, the estimated fault distances in X_D for edge 2-3 are very close. On the other hand, the fault distances computed for the other two edges are rather different (2-1 and 2-4) or equal to zero. Hence, it is concluded that the most likely faulted edge is 2-3. Another accurate way to identify the faulted edge is by comparing the estimated traveling time τ_e given by (26) with the actual traveling time τ_t . As shown in Table I, τ_e and τ_t are similar for two pairs in the edges 2-1 and 2-4. On the other hand, τ_e are completely different than τ_t for the three pairs in the edge 2-3. This is due to the fact that unless F1 occurs at one of the terminal buses, τ_t and τ_e will always be different.

$$\tau_{e(r)} = |t_{a_q}^{(e_i)} - t_{b_v}^{(e_i)}| \quad (26)$$

Identification of the faulted edge is automated in the proposed algorithm by computing the estimated traveling time error $err_{\tau_{e(r)}}$ given by (27), which must satisfy condition (28) for all errors that belong to the same incident edge. For the case of F1, the errors marked in red in Table I satisfy the condition (28) and thus it will identify the faulted section as 2-3.

$$err_{\tau_{e(r)}} \% = \left| \frac{\tau_t^{(e_i)} - \tau_{e(r)}}{\tau_t^{(e_i)}} \right| \times 100 \quad (27)$$

$$err_{\tau_{e(r)}} \% > 0.2 \quad (28)$$

Once the faulty section 2-3 is known, the fault location vector X_D is then extracted from Table I as:

$$X_D = [49.99 \quad 49.99 \quad 49.99] \quad (29)$$

Any outliers are then removed by first taking the **median** of X_D entries, followed by the **mean** of the remaining entries to yield a fault distance of 49.99 km. Note that there are zero distances for branches 2-1 and 2-4. Negative distances are bad data generated by the directed tree, appearing on non-faulted incident edges. Additionally, if condition (28) is not satisfied, the algorithm will identify the fault to be at the fault-closest bus.

F. Differentiating Between Faults and Other Disturbances

The proposed algorithm can differentiate between faults and other disturbances such as switching capacitors, sudden load changes, and high-frequency harmonics. Short-circuits mostly occur along lines, while other disturbances always happen in substation buses. Hence, the disturbance location can serve as one differentiating factor. Besides, the recorded transient voltage at the closest DFR to the disturbance will easily confirm if it is a disturbance or a fault. Additionally, any higher harmonics do not affect the performance of the algorithm because the frequency content of fast transients generated by short-circuits are higher than harmonics whose WTC^2 magnitudes remain insignificant compared to those of faults.

G. Flow Chart of Proposed Fault Location Algorithm

The flowchart of the proposed fault location algorithm is shown in Fig. 10. The algorithm assumes that the Optimal DFR Placement (ODP) algorithm of Section II-A is used to place DFRs in the network. First, ToAs recorded by all DFRs are considered and the entire network is modeled as a weighted undirected graph. If the network is an AC/DC network, first AC and DC networks will be virtually disconnected and a weighted undirected graph is created for each. Then, K-Means clustering is applied to select a subset of DFRs from the entire set to be used for identifying the AC or DC faulted network. The ToAs of the selected DFRs, along with the undirected graph of the faulted network, are used to determine the fault-closest bus. Each branch incident to the fault-closest bus is modeled as a weighted directed tree network to represent the shortest travel times from fault to DFRs, and to compute the matrices of traveling time (τ_a , τ_b) and arrival times (t_a , t_b). The conditions (21) and (22) are then used to obtain the correct ToAs in matrices t_a and t_b . ToAs stored in t_a and t_b are used to determine the vectors X_D for each incident edge and then populate the fault location table. Finally, condition (28) is used to extract the vector X_D corresponding to the real faulted section. Taking the median detects and removes any outliers from X_D , and taking the mean of the rest yields the best fault distance estimate.

III. PRACTICAL IMPLEMENTATION

A. Simulation Model

The AC/DC complex transmission network of Fig. 11, created from the modified IEEE 39 bus system and the CIGRE B4 DC

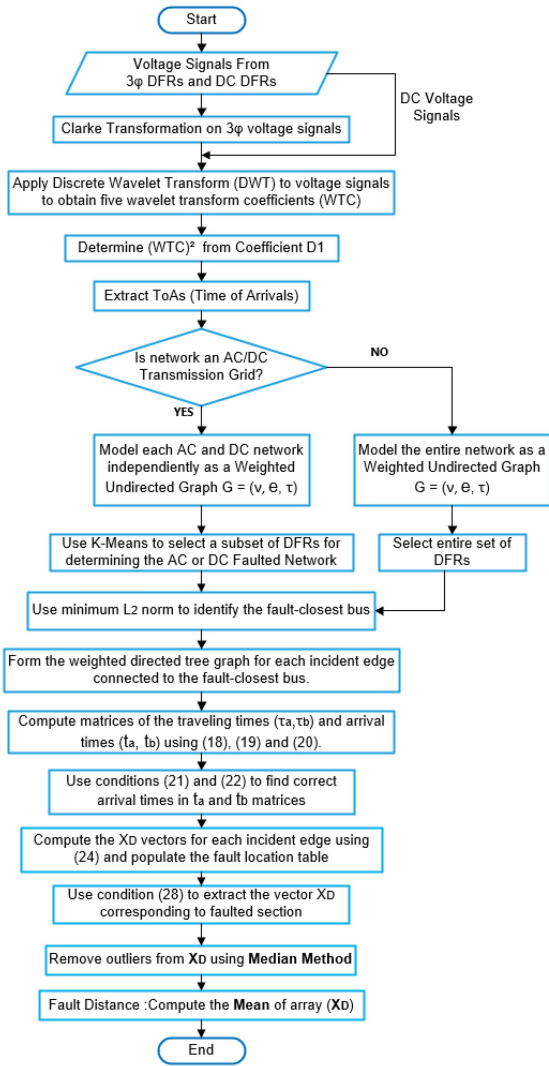


Fig. 10. Flowchart of the proposed fault location algorithm.

grid test systems whose model data for EMT-type simulations studies developed by CIGRE [15], [20] are used to validate the fault location algorithm for hybrid AC/DC transmission grids. Two wind generators of type-III (Doubly-fed induction Generator, DFIG), and type-IV (Full Frequency Converter, FFC), whose detailed model can be found in [21], are connected to the buses 25 and 2. The parameters and settings of these wind turbines can be obtained from [15].

The Voltage Source Converter (VSC) based DC grid system is composed of 2 onshore AC systems-red color (A0, A1, B0, B1, B2, and B3), 4 offshore AC systems-brown color (C1, C2, D1, E1, and F1), 2 DC nodes (B4 and B5), and 3 VSC-DC systems (DCS1, DCS2, and DCS3) of colors light-blue, green and blue as shown in Fig. 11. DCS1 area is a 2-terminal symmetrical monopole HVDC link (+/- 200 KV), DCS2 area is a 4-terminal symmetrical monopole HVDC system (+/- 200 KV), and the DCS3 area is a 5-terminal bipole HVDC meshed grid (+/- 400 KV). DCS3 also contains a DC-DC converter Cb-E1 that connects DCS3 and DCS2 through a transformation ratio of

2. The detailed information of B4 DC grids test systems is presented in [20].

VSC stations are based on Modular Multilevel Converter (MMC) technology, having 201 levels (200 Sub-Module/half arm) in each converter. Several types of MCC models are developed for EMT-type program [22]. However, model 3 presented in [23] is used in the simulation model. Simulation of AC/DC complex transmission system is carried out using EMT-P-RV [24]. Simulated voltage signals captured by DFRs are then used by the proposed algorithm.

The AC and DC networks of AC/DC Complex Transmission System of Fig. 11 are virtually disconnected to create four different networks (AC Network 1, AC Network 2, DC Network 1, and DC Network 2) as shown in Fig. 12. Applying ODP to each network yields 10 AC DFRs in AC Network 1, 2 AC DFRs in AC Network 2, 4 DC DFRs in DC Network 1, and 2 DC DFRs in DC Network 2. Hence, 18 DFRs are required to make the system identifiable for any fault in the network, twelve of which are three-phase AC DFRs (light blue) and the rest are DC DFRs (green) as depicted in Fig. 11. Due to the existence of several overhead line configurations, a 3×10^5 km/s TW speed is used as a good approximation for overhead lines. On the other hand, a 183 524.37 km/s TW speed is used for cables computed using the capacitance and inductance per unit length at each cable section. A sampling frequency of 1 MHz is used to accurately estimate fault distances.

B. Fault Simulations in AC/DC Complex Grid

1) *Pole-to-Ground (P-G) Fault F1 At 25 Km From Bus 46:* A Pole (Positive) to ground fault (F1) shown in Fig. 11 occurs along the 200 km DC overhead line connecting DC buses 47-46, 25 km from bus 46. The fault is simulated assuming a 40Ω fault resistance and a 180 ms fault inception time. The fault-generated voltage signals registered by DFRs are processed to obtain the squared wavelet transform coefficients (WTC^2) from which the Time of Arrivals (ToAs) are extracted. The K-Means clustering with cluster $k = 2$ determined by elbow method is then used to select a DFRs subset. For this case, selecting the blue cluster of DFRs 46, 53, 43, and 52 as shown in Fig. 13 are sufficient to determine the faulted network and accurate fault distance. Note that these selected DFRs are installed in DC Network 1 formed by the DCS2 and DCS3 networks as depicted in Fig. 12. Hence, the proposed algorithm will virtually evaluate the DC Network 1 as separated from the entire AC/DC network. The four ToAs of clustered DFRs shown in Table II are then used to compute the minimum ℓ_2 -norm using (17) to identify the bus 46 as the fault-closest bus as shown in Fig. 14. The incident edges 46-47, 46-41, 46-41, and 46-45 connected to the bus 46 are then selected to identify the edge containing the fault. Note that there are two equal length parallel edges 46-41, which will be evaluated as one edge. The shortest paths from terminal buses of incident edges to clustered DFRs are modeled as weighed directed tree networks to compute using (18), (19) and (20) the matrices of τ_a and τ_b travel time and the t_a and t_b arrival time. The conditions (21) and (22) are used in t_a and t_b to find the correct ToAs. The correct ToAs (non-zero) stored in t_a and t_b can then form

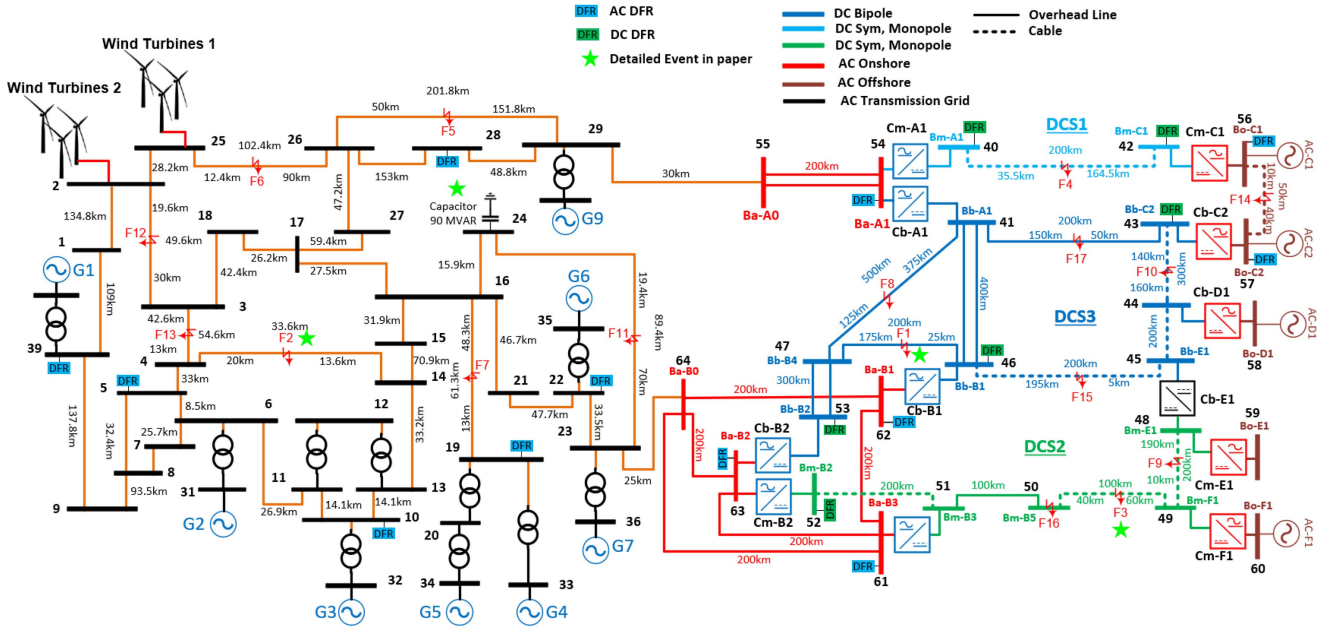


Fig. 11. AC/DC complex transmission system.

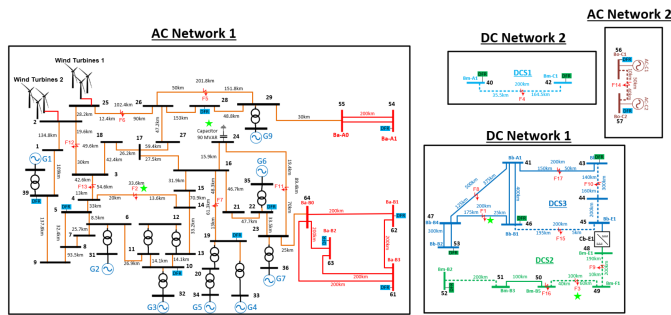


Fig. 12. Virtual disconnections for AC/DC complex system.

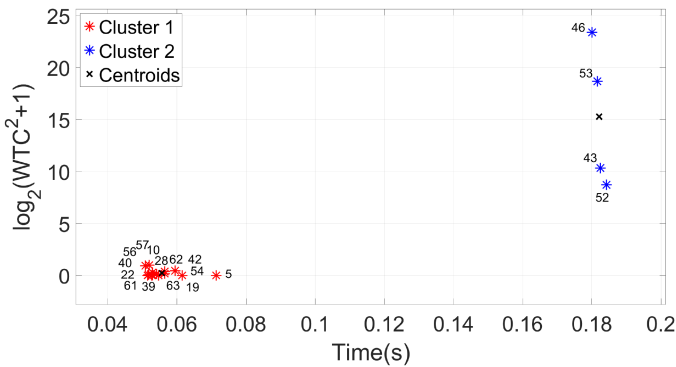


Fig. 13. K-means for F1 fault in DC network.

pairs by selecting columns with the same index at t_a and t_b . These ToAs pairs are then used in (23) and (24) to compute the fault location vector X_D and populate the fault location Table III shown below:

TABLE II
TOA(MS) FOR FAULTS F1, F2, F3, AND CAPACITOR

DFR	$ToAF_1$	DFR	$ToAF_2$	DFR	$ToAF_3$	DFR	ToA_{Cap}
46	180.08	5	185.15	52	186.21	19	182.16
53	181.59	10	185.17	46	187.07	22	182.27
43	182.51	19	185.56	43	188.71	10	182.45
52	183.36	22	185.67	53	188.74	5	182.52
-	-	39	186.03	-	-	28	182.91
-	-	28	186.31	-	-	61	182.95
-	-	-	-	-	-	62	182.95
-	-	-	-	-	-	63	182.95
-	-	-	-	-	-	39	183.4
-	-	-	-	-	-	54	183.84

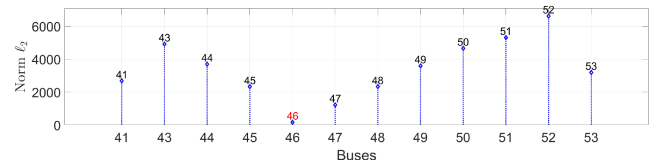


Fig. 14. l_2 -norm for F1 fault in DC network.

TABLE III
FAULT LOCATION TABLE FOR FAULT F1

Edge	t_a	t_b	τ_x	V_e	X_D	τ_e	τ_t	err_{τ_e}
46-41	180.085	181.420	-0.75	300000	-0.22	1334.83	1333.33	0.11
46-41	179.919	181.420	-83.93	300000	-25.18	1501.19	1333.33	12.5
46-41	180.086	181.420	-0.37	300000	-0.11	1334.07	1333.33	0.05
46-45	180.085	181.175	-0.38	183524	-0.07	1090.53	1089.77	0.06
46-45	179.919	181.175	-83.56	183524	-15.34	1256.90	1089.77	15.3
46-46	180.086	181.175	0.37	183524	0.07	1089.04	1089.77	0.06
46-47	180.085	180.585	83.18	300000	24.95	500.30	666.67	24.95
46-47	180.086	180.585	83.93	300000	25.18	498.81	666.67	25.17
46-47	180.086	180.585	83.56	300000	25.07	499.54	666.67	25.06

As shown in Table III, the estimated traveling times τ_e for two arrival time pairs are similar to the actual traveling time τ_t in incident edges 46-41 and 46-45. Other τ_e values are totally

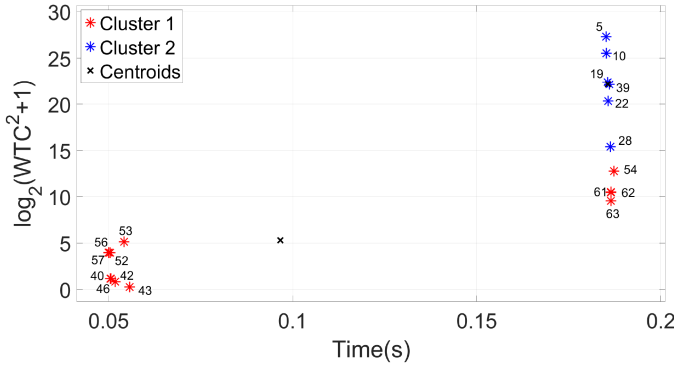


Fig. 15. K-means for F2 fault in AC network.

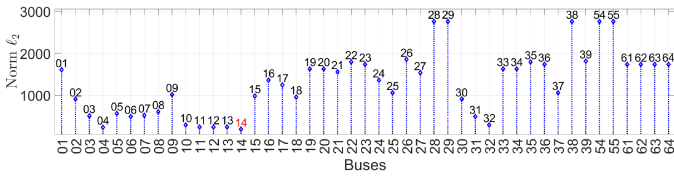


Fig. 16. ℓ_2 -norm for F2 fault in AC network.

different from τ_t for each arrival time pair in edge 46-47. Moreover, the estimated travel time errors err_{τ_e} marked in red satisfy the condition (28). Hence, the faulted edge will be identified as 46-47 and fault location vector X_D will be extracted from Table III as shown below:

$$X_D = [24.95 \quad 25.18 \quad 25.07]$$

Taking the median will detect and remove outliers from X_D . Since there are no outliers in X_D , mean of the entries in X_D will yield the best estimate for the fault distance of 25.067 km. Comparing it with actual distance of 25 km yields an absolute error of 67 m.

2) *DLG Fault F2 At 13.6 Km From Bus 14*: A double-line-to-ground (DLG) fault F2 shown in Fig. 11 happens along the 33.6 km AC overhead line, which connects buses 4-14, 13.6 km from bus 14. The fault is simulated using a 100Ω fault resistance and a 90° fault inception angle, which is set to 184.97 ms. The time of arrivals (ToAs) generated by fault voltage signals are captured by DFRs as shown in Table II. Applying K-Means clustering, the blue cluster of DFRs 5, 10, 19, 22, 39, and 28 shown in Fig. 15 are selected to estimate the accurate fault distance. These selected DFRs are placed in the AC Network 1 as shown in Fig. 12. While DFRs 54, 61, 62, and 63 also belong to the AC Network 1, K-Means clustering places them in the red cluster due to their distance from fault F2. Only the six ToAs of the blue cluster shown in Table II are used to identify bus 14 as the fault-closest bus as well as shown in Fig. 16. The incident edges 14-4, 14-13, and 14-15 to bus 14 are then selected and the shortest traveling time routes from their terminal buses to clustered DFRs are modeled as weighted directed tree networks to compute using (18), (19), and (20) the traveling time (τ_a and τ_b) and arrival time (t_a and t_b) matrices. The conditions (21) and (22) are utilized in t_a and t_b to filter the correct ToAs. Selecting columns of equal index at t_a and t_b , ToA pairs can then be formed

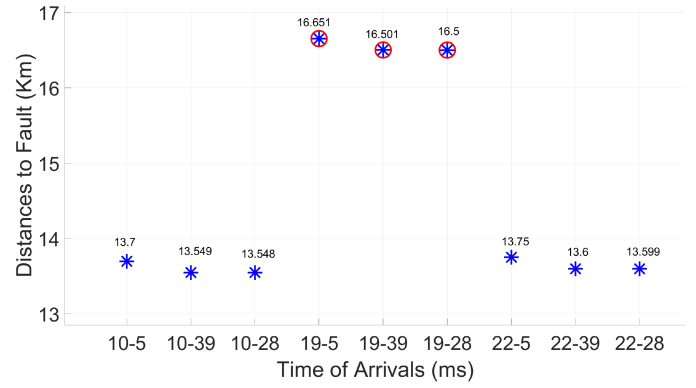


Fig. 17. Gross errors detected by median.

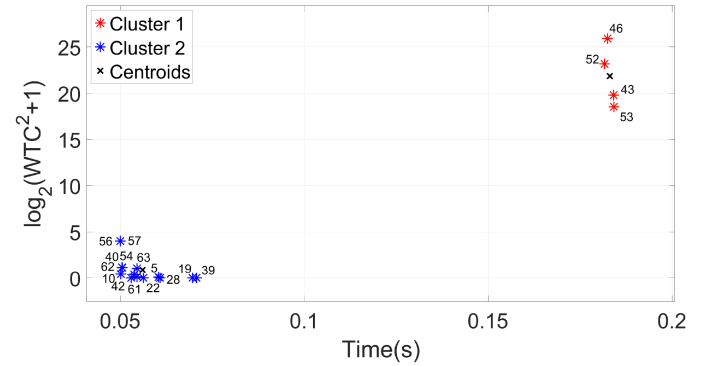


Fig. 18. K-means for F3 fault in DC network.

to compute the fault location table. For an issue of space only the fault location vector X_D extracted from the table is shown below:

$$X_D = [13.7 \quad 13.54 \quad 13.548 \quad 13.652 \quad 13.501 \quad 13.5 \quad 13.75 \quad 13.6 \quad 13.59]$$

Using the median method does not detect any outliers in X_D . Finally, calculating the mean of X_D will yield the fault distance of 13.6 km, and comparing it with the actual distance of 13.6 km will produce an absolute error of 0.0 m.

3) *Performance in the Presence of Gross Errors in ToAs*: Consider the same fault F2 and let DFRs 19, 53 and 62 have gross errors of $20 \mu s$, $25 \mu s$ and $20 \mu s$ in their ToAs. Applying K-Means clustering excludes DFRs 53 and 62 and selects the six DFRs marked in blue in Fig. 15. Hence, only the error of DFR 19 can impact fault estimation accuracy. However, taking the median of X_D will remove the three gross errors marked in red in Fig. 17. Note that these outliers are formed by DFR pairs 19-5, 19-39, and 19-28.

The median removes the outliers and calculating the mean of the remaining entries will yield the fault distance of 13.62 km, which has an absolute error of 20 m.

4) *Pole(+)-to-Pole(-) Fault F3 in DC Cable At 40 Km From Bus 50*: Pole (Positive) to pole (Negative) fault F3 shown in Fig. 11 occurs along the 100 km DC cable, which connects buses 50-49, 40 km from bus 50. The fault is simulated assuming a 185 ms fault inception time. Using K-Means, the red clusters of DFRs 52, 46, 43, and 53 shown in Fig. 18 are selected to

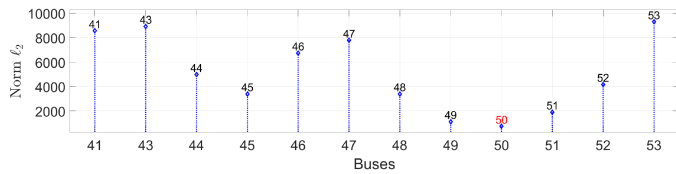
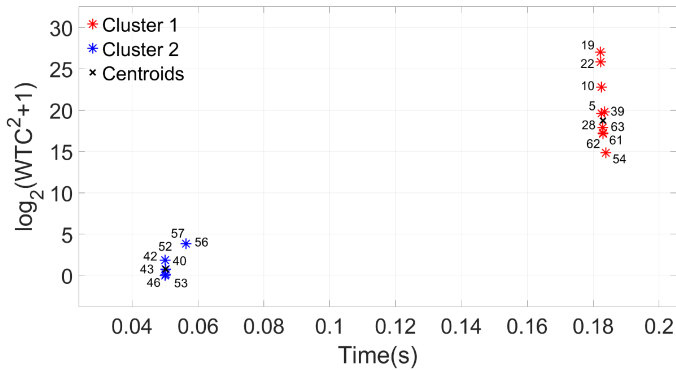

 Fig. 19. l_2 -norm for F3 fault in DC network.


Fig. 20. K-means for capacitor switching at bus 24.

estimate the accurate fault distance. These selected DFRs are in DC network 1 as shown in Fig. 12. Hence, the DC Network 1 will be evaluated as an independent network to compute the fault distance. The ToAs of clustered DFRs are shown in Table II. The minimum l_2 -norm identifies bus 50 as the fault-closest bus as shown in Fig. 19. Then, incident branches 50-51 and 50-49 are selected to compute the arrival time matrices t_a and t_b and the fault location vectors X_D for each incident edge. To avoid redundancy only the vector X_D corresponding to the faulted section extracted from the fault location table is shown below.

$$X = [40.038 \quad 39.962 \quad 40.007]$$

The median does not detect any outlier, and calculating the mean yields a fault distance of 40.002 km. Comparing it with the actual distance of 40 km yields an absolute error of 2 m. Even though the fault occurs in the cable section, the proposed algorithm is able to estimate the fault location accurately, demonstrating the robustness of the method for line-cable hybrid networks.

5) *Differentiating Between Faults and Switching Events:* Transients generated by switching of capacitors or load/generation can be differentiated from fault transients by their location. As an example, consider switching of a 345KV, 90 MVAR capacitor at bus 24 as shown in Fig. 11. The switch closing angle is 30° (or 181.9 ms). The K-Means clustering yields the cluster of DFRs 19, 22, 10, 5, 39, 28, 63, 62, 61, and 54 marked in red in Fig. 20, and placed in the AC Network 1 of Fig. 12. The ToAs of clustered DFRs shown in Table II are then used to identify bus 24 as the fault-closest bus. Then, the fault distance vector X_D is computed as:

$$X_D = [0.09 \ 0 \ 0.05 \ 0.1 \ 0.04 \ 0.04 \ 0 \ 0 \ 0 \ 0.1 \ \dots \ 0 \ 0]$$

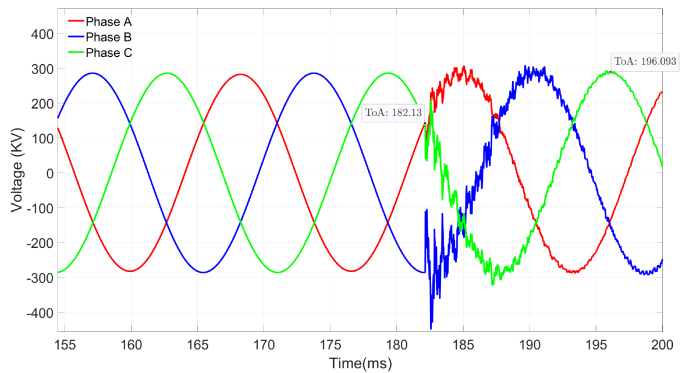


Fig. 21. Voltage transients of capacitor switching at bus 24.

 TABLE IV
 FAULT LOCATION ERRORS AT AC/DC SYSTEM

Fault	Location	Rf	Fault Angle	Fault Type	Err (m)
F1-DC	12.5% L_{46-47}	50Ω	-	$p^{(+)} - g$	67
F2-AC	40.47% L_{14-4}	150Ω	135°	AC-g	0.0
F3-DC	40% L_{50-49}	-	-	$p^{(+)} - p^{(-)}$	2
F4-DC	17.75% L_{40-42}	45Ω	-	$p^{(-)} - g$	35.8
F5-AC	24.7% L_{26-29}	20Ω	45°	A-g	12.5
F6-AC	12.1% L_{25-26}	200Ω	90°	B-g	10.25
F7-AC	21.2% L_{19-16}	160Ω	135°	ABC	9.5
F8-DC	25% L_{47-41}	40Ω	-	$p^{(+)} - g$	42.3
F9-DC	5% L_{49-48}	55Ω	-	$p^{(+)} - g$	55
F10-DC	46.67% L_{43-44}	-	-	$p^{(+)} - p^{(-)}$	15.5
F11-AC	21.7% L_{24-23}	90Ω	45°	C-g	7.5
F12-AC	39.51% L_{2-3}	75Ω	45°	AC	14.8
F13-AC	23.8% L_{4-3}	150Ω	150°	A-g	17.8
F14-AC	20% L_{56-57}	190Ω	90°	AB	10.5
F15-DC	2.5% L_{45-46}	-	-	$p^{(+)} - p^{(-)}$	34.3
F16-DC	Bus 50	15Ω	-	$p^{(+)} - g$	24.8
F17-DC	25% L_{43-41}	-	-	$p^{(+)} - p^{(-)}$	45.5

The mean of X_D yields a fault distance of 0.032 km, which is very close to bus 24. This result implies the possibility of a switching event instead of a short-circuit. It can be readily verified by observing the recorded voltage transient by DFR 19, the closest to the location of the disturbance. As seen in Fig. 21, the 3-phase voltage transients last about 13.9 ms and return back to steady-state, verifying it as a switching event.

C. Summary of Simulated Fault Location Cases.

AC and DC fault scenarios as depicted in Fig. 11 are simulated for the AC/DC Complex Transmission System using different fault conditions in the presence of non-transposed AC lines, DC lines, IBPSs, and VSC-HVDCs. Simulation results give maximum and average absolute errors of 67 m and 23.82 m as shown in Table IV. The obtained results confirms that the proposed algorithm can determine accurately the fault location in DC and AC transmission grids.

IV. CONCLUSION

This paper presents a robust and precise fault location algorithm for hybrid AC/DC transmission grids containing DERs and HVDC lines. It can locate faults irrespective of their occurrence in the DC or AC parts of the network. An optimal strategy for

placing DFRs is also developed and implemented. Detailed description of the fault location algorithm and underlying methodology are provided with tutorial examples. An AC/DC complex transmission system is used to illustrate the performance of proposed method under different fault scenarios and locations.

REFERENCES

- [1] A. D. Filomena, R. H. Salim, M. Resener, and A. S. Bretas, "Ground distance relaying with fault-resistance compensation for unbalanced systems," *IEEE Trans. Power Del.*, vol. 23, no. 3, pp. 1319–1326, Jul. 2008.
- [2] S. Paladhi and A. K. Pradhan, "Adaptive distance protection for lines connecting converter-interfaced renewable plants," *IEEE Trans. Emerg. Sel. Topics Power Electron.*, vol. 9, no. 6, pp. 7088–7098, Dec. 2021.
- [3] C. Galvez and A. Abur, "Fault location in active distribution networks containing distributed energy resources (DERs)," *IEEE Trans. Power Del.*, vol. 36, no. 5, pp. 3128–3139, Oct. 2021.
- [4] D. Tzelepis, G. Fusiek, A. Dyško, P. Niewczas, C. Booth, and X. Dong, "Novel fault location in MTDC grids with non-homogeneous transmission lines utilizing distributed current sensing technology," *IEEE Trans. Smart Grid*, vol. 9, no. 5, pp. 5432–5443, Sep. 2018.
- [5] O. M. K. K. Nanayakkara, A. D. Rajapakse, and R. Wachal, "Traveling-wave-based line fault location in star-connected multiterminal HVDC systems," *IEEE Trans. Power Del.*, vol. 27, no. 4, pp. 2286–2294, Oct. 2012.
- [6] O. M. K. K. Nanayakkara, A. D. Rajapakse, and R. Wachal, "Location of DC line faults in conventional HVDC systems with segments of cables and overhead lines using terminal measurements," *IEEE Trans. Power Del.*, vol. 27, no. 1, pp. 279–288, Jan. 2012.
- [7] S. Azizi, M. Sanaye-Pasand, M. Abedini, and A. Hasani, "A traveling-wave-based methodology for wide-area fault location in multiterminal DC systems," *IEEE Trans. Power Del.*, vol. 29, no. 6, pp. 2552–2560, Dec. 2014.
- [8] F. V. Lopes, "Settings-free traveling-wave-based earth fault location using unsynchronized two-terminal data," *IEEE Trans. Power Del.*, vol. 31, no. 5, pp. 2296–2298, Oct. 2016.
- [9] Y. Xi, Z. W. Li, X. Zeng, X. Tang, X. Zhang, and H. Xiao, "Fault location based on travelling wave identification using an adaptive extended Kalman filter," *Iet Gener. Transmiss. Distrib.*, vol. 12, pp. 1314–1322, 2017.
- [10] C. Zhang, G. Song, T. Wang, and L. Yang, "Single-ended traveling wave fault location method in DC transmission line based on wave front information," *IEEE Trans. Power Del.*, vol. 34, no. 5, pp. 2028–2038, Oct. 2019.
- [11] L. Kong and H. Nian, "Fault detection and location method for mesh-type DC microgrid using pearson correlation coefficient," *IEEE Trans. Power Del.*, vol. 36, no. 3, pp. 1428–1439, Jun. 2021.
- [12] M. Monadi, C. Koch-Ciobotaru, A. Luna, J. I. Candela, and P. Rodriguez, "A protection strategy for fault detection and location for multi-terminal MVDC distribution systems with renewable energy systems," in *Proc. Int. Conf. Renewable Energy Res. Appl.*, 2014, pp. 496–501.
- [13] E. C. M. Maritz, J. M. Maritz, and M. Salehi, "A travelling wave-based fault location strategy using the concepts of metric dimension and vertex covers in a graph," *IEEE Access*, vol. 9, pp. 155815–155825, 2021.
- [14] C. Galvez and A. Abur, "Fault location in meshed and active power distribution networks," in *Proc. IEEE Madrid PowerTech*, 2021, pp. 1–6.
- [15] CIGRE, "Power system test cases for EMT-type simulation studies," Accessed: Feb. 3, 2018. [Online]. Available: <https://e-cigre.org/publication/736-power-system-test-cases-for-ent-type-simulation-studies>
- [16] J. R. Marti, "Accurate modelling of frequency-dependent transmission lines in electromagnetic transient simulations," *IEEE Trans. Power App. Syst.*, vol. PAS- 101, no. 1, pp. 147–157, Jan. 1982.
- [17] H. W. Dommel, *EMTP Theory Book. Microtran Power System Analysis Corporation*. Wuhan, China: Sci. Res., 1996.
- [18] I. Daubechies, *Ten Lectures on Wavelets*. Philadelphia, PA, USA: SIAM, 1992, vol. 61.
- [19] K. P. Murphy, *Machine Learning: A Probabilistic Perspective*. Cambridge, MA, USA: MIT press, 2012.
- [20] S. Denetiere, B. Bruned, H. Saad, and E. Lemieux, "Task separation for real-time simulation of the CIGRE DC grid benchmark," in *Proc. Power Syst. Computation Conf.*, 2018, pp. 1–7.
- [21] U. Karağaç et al., "A generic EMT-type model for wind parks with permanent magnet synchronous generator full size converter wind turbines," *IEEE Power Energy Technol. Syst. J.*, vol. 6, no. 3, pp. 131–141, Sep. 2019.
- [22] H. Saad et al., "Modular multilevel converter models for electromagnetic transients," *IEEE Trans. Power Del.*, vol. 29, no. 3, pp. 1481–1489, Jun. 2014.
- [23] H. Saad, S. Denetiere, and J. Mahseredjian, "On modelling of MMC in EMT-type program," in *Proc. IEEE 17th Workshop Control Model. Power Electron.*, 2016, pp. 1–7.
- [24] J. Mahseredjian, S. Denetiere, L. Dubé, B. Khodabakhchian, and L. Gérin-Lajoie, "On a new approach for the simulation of transients in power systems," *Electric Power Syst. Res.*, vol. 77, no. 11, pp. 1514–1520, 2007. [Online]. Available: <https://www.sciencedirect.com/science/article/pii/S0378779606002094>

Cesar Galvez (Graduate Student Member, IEEE) received the B.S. degree from Callao University, Callao, Peru, in 2005, and the M.S. degree from Northeastern University, Boston, MA, USA, where he is currently working toward the Ph.D. degree in power system with specialization in control and power system modeling.

Ali Abur (Fellow, IEEE) received the B.S. degree in electrical engineering from Orta Doğu Teknik Üniversitesi, Ankara, Turkey, and the M.S. and Ph.D. degrees from The Ohio State University, Columbus, OH, USA. He is currently a Professor with Electrical and Computer Engineering Department, Northeastern University, Boston, MA, USA.